Surface Review and Letters, Vol. 9, No. 2 (2002) 983–987

POLARIZATION DEPENDENCE OF RESONANT SOFT X-RAY EMISSION SPECTRA IN Ce COMPOUNDS

M. WATANABE and Y. HARADA
RIKEN/SPring-8, Kouto 1-1-1, Mikazuki, Sayo, Hyogo 679-5148, Japan

M. NAKAZAWA
JASRI/SPring-8, Kouto 1-1-1, Mikazuki, Sayo, Hyogo 679-5198, Japan

Y. ISHIWATA and R. EGUCHI
The Institute for Solid State Physics, University of Tokyo, Kashiwanoha, Kashiwa, Chiba 277-8581, Japan

T. TAKEUCHI
Faculty of Science, Science University of Tokyo, Kagurazaka, Shinjuku, Tokyo 162-8601, Japan

A. KOTANI
The Institute for Solid State Physics, University of Tokyo, Kashiwanoha, Kashiwa, Chiba 277-8581, Japan

S. SHIN
The Institute for Solid State Physics, University of Tokyo, Kashiwanoha, Kashiwa, Chiba 277-8581, Japan
RIKEN/SPring-8, Kouto 1-1-1, Mikazuki, Sayo, Hyogo 679-5148, Japan

The electronic structures of Ce compounds have been investigated by means of resonant soft X-ray emission spectroscopy (RXES) excited at resonant energy range of Ce $3d \rightarrow 4f$ absorption. Polarization dependence of the RXES shows information on concerning electronic states. In CeO_2, the Ce $4f \rightarrow 3d$ RXES spectra are interpreted as electronic structures hybridized between $4f^0$ and $4f^1\underline{v}$ states. Peaks appearing in the spectra are attributed to bonding, nonbonding, and antibonding states between those states, while the spectra of $CeRh_3$ cannot be explained by only using the hybridization between $4f^0$ and $4f^1\underline{v}$ states. The spectra have large broad Raman peak, especially when the excitation photon energy is set at satellite of Ce $3d \rightarrow 4f$ absorption. We attribute the origin of the broad Raman peak to hybridization states involving electron–hole pairs.

1. Introduction

The electronic structures of Ce compounds have attracted attention due to anomalous physical properties, which are mainly caused by highly correlated Ce $4f$ electrons. It is well known that the Ce $4f$ and the valence band hybridize each other and the hybridization causes the interesting electronic and magnetic properties of the compounds. At first, CeO_2 was investigated by using X-ray photoelectron spectroscopy (XPS), and the spectrum was analyzed by cluster model calculation.[1] The calculation revealed that the ground state is described by a linear combination of $4f^0$ and $4f^1\underline{v}$ states, where $\underline{v}$ represents a ligand hole. XPS of valence band (v-XPS) and bremsstrahlung isochromat spectroscopy (BIS) were also measured for CeO_2.[2] Kotani *et al.*

interpreted the spectra using the impurity Anderson model (IAM).[3]

Butorin *et al.* made Ce $4f \rightarrow 3d$ RXES measurements on CeO_2 in a polarized geometry.[4] The RXES spectra of CeO_2 were calculated using the IAM and it was revealed that peaks of RXES come from bonding, nonbonding, and antibonding states caused by the hybridization between Ce $4f$ orbital and O $2p$ band.[5–8] Furthermore, polarization dependence study of RXES was measured in TiO_2.[9] The differences of the RXES spectra by polarization dependence study involve information about symmetry of concerning electronic states.

The purpose of this paper is to make measurements of the polarization dependence of Ce $4f \rightarrow 3d$ RXES in Ce compounds, particularly in CeO_2 and $CeRh_3$. CeO_2 has a strongly hybridized $4f$ state between $4f^0$ and $4f^1(\underline{v})$ configurations. It is convenient to study the electronic structure using polarization dependence of RXES as a typical example. Thereafter, $CeRh_3$ is also one of the strongly hybridized Ce compounds, but one of the intermetallic compounds. It might be possible that the spectra are interpreted as the same argument as of CeO_2. On the other hand, if there are any differences between those spectra, the differences must have important information about the metallic property. The RXES spectra of CeO_2 and $CeRh_3$ are analyzed by the IAM calculation.

2. Experimental

The experiments have been accomplished at the Photon Factory. The beamline is an undulator beamline BL-2C.[10,11] The soft X-ray (SX) spectrometer[12] is designed on the Rowland-mount condition. A ray-trace simulation shows the energy resolution of about $E/dE = 1000$. The base pressure of the measurement chamber is about 2×10^{-10} Torr.

The measurement chamber with the SX spectrometer is rotatable along the center axis of the chamber in order to execute measurements of the polarization dependence. By the rotation, the spectrometer moves between vertical and horizontal locations. Those locations satisfy experimental arrangements of polarized and depolarized geometries.[9,13]

A single-crystal sample of CeO_2 and $CeRh_3$ was scraped by a diamond file in a sample preparation chamber under an ultrahigh vacuum of 1×10^{-10} Torr. The scraped sample was transferred into the measurement chamber *in situ*. The measurements for CeO_2 were done at room temperature, and the measurements for $CeRh_3$ were done at about 40 K.

3. Model and Formalism

For CeO_2, we consider a system which consists of a filled valence band (an oxygen $2p$ band), an empty Ce $4f$ level, and an occupied core level (Ce $3d$ level). We take into account the hybridization V between the $4f$ and valence band states, and the intra-atomic Coulomb interaction U_{ff} between $4f$ electrons. In the intermediate state of $4f \rightarrow 3d$ RXES, the $4f$ level is pulled down by the core hole potential $-U_{fc}$.

We assume that the system is in the SO_3 symmetry, which is a good approximation in the analysis of high energy spectroscopy of CeO_2.[3,14,15,7] Then the Hamiltonian of the system is given by

$$H = H_1 + H_2 \,, \tag{1}$$

where

$$\begin{aligned} H_1 = & \sum_{k,\nu} \varepsilon_v(k) a_v^\dagger(k,\nu) a_v(k,\nu) \\ & + \varepsilon_f^0 \sum_{\nu} a_f^\dagger(\nu) a_f(\nu) + \varepsilon_d \sum_{\mu} a_d^\dagger(\mu) a_d(\mu) \\ & + U_{ff} \sum_{\nu > \nu'} a_f^\dagger(\nu) a_f(\nu) a_f^\dagger(\nu') a_f(\nu') \\ & + \frac{V}{\sqrt{N}} \sum_{k,\nu} [a_v^\dagger(k,\nu) a_f(\nu) + a_f^\dagger(\nu) a_v(k,\nu)] \\ & - U_{fc} \sum_{\mu,\nu} a_d(\mu) a_d^\dagger(\mu) a_f^\dagger(\nu) a_f(\nu) \,. \end{aligned} \tag{2}$$

Here, H_1 describes the IAM with the valence band level $\varepsilon_v(k)$, the $4f$ level ε_f^0, and the $3d$ level ε_d, and $a_v^\dagger(k,\nu)$, $a_f^\dagger(\nu)$, and $a_d^\dagger(\mu)$ are the electron creation operators in these states. k denotes the index of energy level in the valence band, and ν and μ denote the combined indices to specify both the spin and orbital degeneracies of the f and d states, respectively. H_2 represents multiplet coupling effects, though the explicit form is not given here. The Hamiltonian H is diagonalized using the basis states of $4f^0$, $4f^1\underline{v}$, and $4f^2\underline{v}^2$ configurations for the initial and final states of RXES.

Using the formula of the coherent second-order optical process, the polarization-dependent spectrum

of the $4f \rightarrow 3d$ RXES is given by

$$F(\Omega,\omega) = \sum_q \sum_f \left| \sum_m \frac{\langle f|C_q^{(1)}|m\rangle\langle m|C_0^{(1)}|g\rangle}{E_g + \Omega - E_m - i\Gamma_m} \right|^2 A_q \times \delta(E_g + \Omega - E_f - \omega)\,, \quad (3)$$

where $|g\rangle$ is the ground state of H with energy E_g, and $|m\rangle$ and $|f\rangle$ are intermediate and final states with energies E_m and E_f, respectively. The polarization-dependent factor A_q is given in Refs. 8 and 13.

We use the following parameters for CeO_2: $V = 0.9$, $\varepsilon_f^0 - \varepsilon_v^0 = 2.5$, $U_{ff} = 8.0$, $U_{fc} = 12.0$, $W = 1.3$, where ε_v^0 and W are the center and the width of the valence band, and the core hole lifetime broadening $\Gamma_m = 0.3$ and 0.4 for $3d_{5/2}$, $3d_{3/2}$, respectively, in units of eV. The calculated line spectra are convoluted by the Gaussian function with the width (FWHM) 1.0 eV to represent the experimental resolution.

4. Results and Discussions

4.1. *CeO_2*

Figure 1 shows a comparison between the experimental and calculated results of the RXES spectra for CeO_2. The abscissa indicates the energy loss. The letters denote the excitation photon energies. For simplicity, only the spectra excited around the M_4 XAS peak are displayed. Thick solid lines and thick hatched lines are the experimental results, and thin lines are the calculated ones.

Each experimental spectrum of the polarized geometry has the elastic scattering peak and some inelastic scattering peaks. The inelastic scattering peaks seem to be composed of two Raman scattering peaks with constant energies of 4 and 6 eV respectively (spectra A and D). While the intensity of the elastic peak drastically changes depending on the incident photon energy, the intensities of the 4 and 6 eV Raman peaks are always weak except when the excitation energy is set around the absorption satellites.

The ground state is the bonding state mainly composed of $4f^0$ and $4f^1\underline{v}$ configurations, because the energy of the $4f^2\underline{v}^2$ configuration is much higher than those of $4f^0$ and $4f^1\underline{v}$. The antibonding state is also mainly composed of $4f^0$ and $4f^1\underline{v}$ configurations. In addition, there exist many $4f^1\underline{v}$ nonbonding charge transfer states, whose energies are located between the bonding and antibonding states. A schematic view of these energy levels is drawn in Fig. 2. After consideration of the energy diagram, we attribute the 4 and 6 eV Raman peaks to the nonbonding and antibonding states.

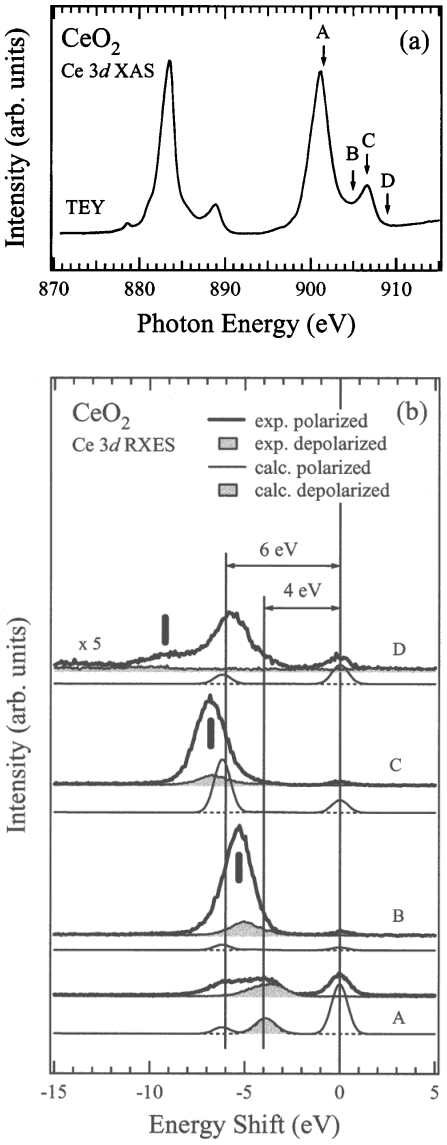

Fig. 1. XAS and RXES spectra of CeO_2. (a) Ce $3d$ XAS spectrum measured by total electron yield. Letters and arrows above the XAS spectrum represent incident photon energies for the respective RXES spectra. (b) Ce $4f \rightarrow 3d$ RXES spectra of CeO_2. The experimental results are drawn by thick solid lines and thick hatched lines for the spectra of polarized and depolarized geometries, respectively. Thick vertical bars represent fluorescence-like spectral peaks. The calculated results are drawn by thin solid lines and hatched lines.

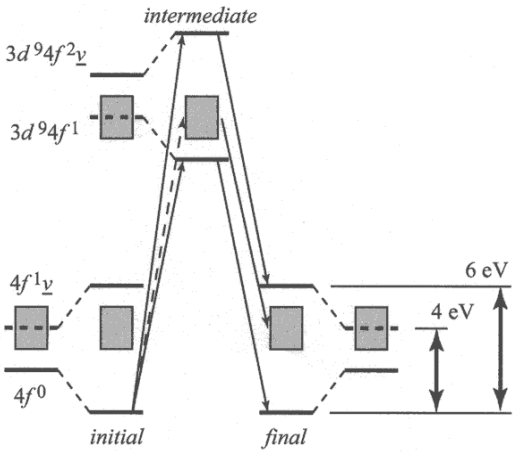

Fig. 2. Energy diagram of $4f$ electronic states hybridized with valence band. The ground state is the bonding state between $4f^0$ and $4f^1\underline{v}$.

By the polarization dependence of RXES, we found that the 4 eV inelastic scattering peak appears in both experimental geometries, and that the elastic scattering peak and 6 eV peak appear only in the polarized geometry. This is experimental evidence of the assignment of the elastic, 4 and 6 eV peaks to the bonding, nonbonding, and antibonding states, respectively.[13]

The calculated and experimental results of the spectrum A are in good agreement with each other, especially for the energy separation of 4 and 6 eV. However, the agreement for the spectra B and C is not good enough. We denote that the differences come from the existence of a fluorescence-like peak in the experimental results. The emitted photon energy of the fluorescence-like peak is almost independent of the incident photon energy. Therefore, the fluorescence-like peak is superposed on the 4 and 6 eV Raman spectra. Thick vertical lines in the figure represent fluorescence-like peaks. On the other hand, the fluorescence-like spectrum is absent in our calculation.

4.2. *$CeRh_3$*

Figure 3 shows the $CeRh_3$ RXES spectra resonantly excited at the excitation energy around the Ce $3d \rightarrow 4f$ absorption threshold. The uppermost spectrum shows the Ce $3d \rightarrow 4f$ XAS spectrum by TEY measurement. Letters and arrows represent incident photon energies for the respective RXES spectra.

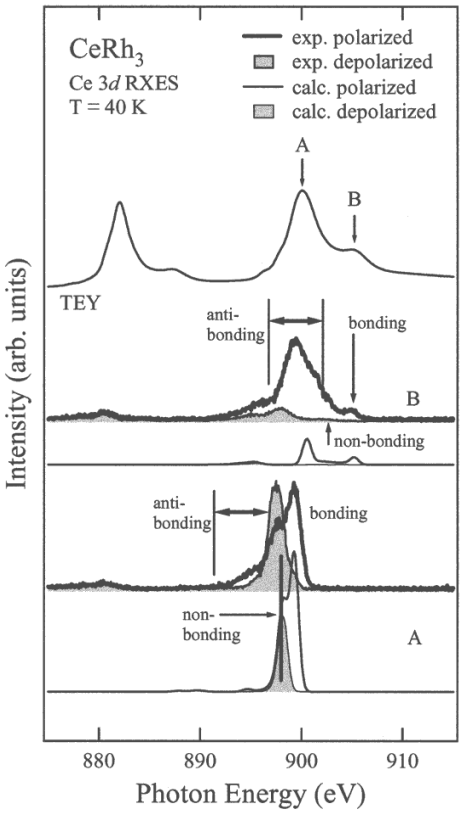

Fig. 3. XAS and RXES spectra of $CeRh_3$. Letters and arrows above the XAS spectrum represent incident photon energies for the respective RXES spectra. The experimental results of RXES are drawn by thick solid lines and thick hatched lines, and the calculated results are drawn by thin lines. The antibonding state appears as a broad peak especially in the spectrum B.

There is an apparent difference between the RXES spectra of polarized and depolarized geometries. In the spectrum A, the experimental result of the polarized geometry has three-peak structure, and there is single-peak structure for the depolarized geometry. The energy of the single peak is about 2 eV from the elastic scattering peak. According to the analysis, the spectrum A is well reproduced by the calculation. By the same argument as for CeO_2, the three peaks are attributed to the bonding, nonbonding, and antibonding states. The polarization dependence of A is very similar to the result for CeO_2. However, the antibonding peak seems to be broad.

On the other hand, the spectrum B of the polarized geometry has a large broad peak and a small elastic scattering peak. In the spectrum of the

depolarized geometry, there is a weak peak beside the photon energy of the incident beam. The energy loss of the weak peak is about 2 eV. By the same discussion as for the spectrum A, we want to attribute the elastic scattering, 2 eV, and large broad peaks to the bonding, nonbonding, and antibonding states.

The problem is that the Raman peak width of the antibonding state is much broader than the width of the elastic scattering peak. We consider that the broadness of the antibonding state comes from the contribution of states possessing electron–hole pairs; $4f^0c^1\underline{v}$ and $4f^1c^1\underline{v}^2$ for one electron–hole pair,[16] where the c represents an electron in the conduction band. While CeO_2 is an insulator, $CeRh_3$ is metallic compounds. Therefore, we cannot always ignore the effects of the electron–hole pairs contributing to the hybridization. The other spectroscopies do not deduce information about the electron–hole pairs. The spectra of the other study are interpreted using the IAM without the electron–hole pairs. However, we have to consider the contribution of the electron–hole pairs in order to analyze the RXES spectra.

5. Conclusion

Polarization dependence studies of RXES in CeO_2 and $CeRh_3$ show the hybridized electronic structures. In the case of CeO_2, the elastic and inelastic peaks are attributed to the bonding, nonbonding, and antibonding states concerning the $4f^0$ and $4f^1\underline{v}$ configurations. In addition, the peaks show the polarization dependence of the incident photon. While the bonding and the antibonding states appear only in the polarized geometry, the nonbonding state exists in both geometries. The calculation using the single IAM can reproduce the experimental data. In the case of $CeRh_3$, the spectra have a broad peak as the antibonding state. This broadness comes from hybridization with states including electron–hole pairs.

Acknowledgments

Many staffers of the Photon Factory supported us in accomplishing the measurements. We would like to thank them for their help. This work is partly supported by a Grant-in-Aid for Scientific Research from the Ministry of Education, Culture, Sports, Science and Technology.

References

1. A. Fujimori, *Phys. Rev.* **B28**, 2281 (1983).
2. E. Wuilloud, B. Delley, W.-D. Schneider and Y. Baer, *Phys. Rev. Lett.* **53**, 202 (1984).
3. A. Kotani, H. Mizuta, T. Jo and J. C. Parlebas, *Solid State Commun.* **53**, 805 (1985).
4. S. M. Butorin, D. C. Mancini, J.-H. Guo, N. Wassdahl and J. Nordgren, *J. Alloys Comp.* **225**, 230 (1995).
5. S. M. Butorin, D. C. Mancini, J.-H. Guo, N. Wassdahl, J. Nordgren, M. Nakazawa, S. Tanaka, T. Uozumi, A. Kotani, Y. Ma, K. E. Myano, B. A. Karlin and D. K. Shuh, *Phys. Rev. Lett.* **77**, 574 (1996).
6. M. Nakazawa, S. Tanaka, T. Uozumi and A. Kotani, *J. Electron Spectrosc. Relat. Phenom.* **79**, 183 (1996)
7. M. Nakazawa, S. Tanaka, T. Uozumi and A. Kotani, *J. Phys. Soc. Jpn.* **65**, 2303 (1996).
8. M. Nakazawa, H. Ogasawara and A. Kotani, *J. Phys. Soc. Jpn.* **69**, 4071 (2000).
9. Y. Harada, T. Kinugasa, R. Eguchi, M. Matsubara, A. Kotani, M. Watanabe, A. Yagishita and S. Shin, *Phys. Rev.* **B61**, 12854 (2000).
10. M. Watanabe, A. Toyoshima, Y. Azuma, T. Hayaishi, Y. Yan and A. Yagishita, *Proc. SPIE* **3150**, 58 (1997).
11. M. Watanabe, A. Toyoshima, J. Adachi and A. Yagishita, *Nucl. Instrum. Methods* **A467–468**, 512 (2001).
12. Y. Harada, H. Ishii, M. Fujisawa, Y. Tezuka, S. Shin, M. Watanabe, Y. Kitajima and A. Yagishita, *J. Synchrotron Rad.* **5**, 1013 (1998).
13. M. Watanabe *et al.*, unpublished.
14. T. Jo and A. Kotani, *J. Magn. Magn. Mat.* **70**, 394 (1987); *Phys. Rev.* **B38**, 830 (1988); *J. Magn. Magn. Mat.* **76&77**, 361 (1988); *J. Phys. Soc. Jpn.* **57**, 2288 (1988).
15. A. Kotani, H. Ogasawara, K. Okada, B. T. Thole and G. A. Sawatzky, *Phys. Rev.* **B40**, 65 (1989).
16. M. Nakazawa *et al.*, unpublished.